



BACHELOR THESIS

MINT Faculty
Department of Physics
Physics course of study

# Characterization of optical components to determine the efficiency of the ALPS II TES detector

submitted by

*Jan Wiesenmüller*

Mat. Nr.: 7235627

22.12.2022

supervised by

First assessor: Dr. Manuel Meyer

Second assessor: Dr. Gulden Othman

Supervision: Dr. Gulden Othman

# Contents

**Abstract**

This bachelor thesis describes the characterization of the optical components to determine the efficiency of the Any Light Particle Search II TES detector.
This thesis is performed and written in the context of the (ALPS II) experiment, which is located on the premises of the Deutsches Elektronen-Synchrotron (DESY) research center. The ALPS II experiment is designed to detect weakly interacting particles, known as weakly interacting sub-eV particles (WISP), and thus for example the existence of axions. These particles are considered possible candidates for dark matter.
To detect axions, a laser beam is sent through a magnetic field, where the photonsA wall blocks the unconverted photons, since they have extremely weak interactions. The axions can then propagate to a second magnetic region where they are converted back into photons. The axions are then transferred to a second magnetic field where they are converted back into photons. These converted photons are measured by a transition edge sensor (TES). Since the expected rate of converted axions is very low, the losses in the TES must be determined.
For this purpose, an experimental setup is used in which a laser beam, with the same wavelength as that of the expected photons, is directed with a beam splitter to the TES and a photodiode for reference measurement of the power. Since the photodiode has a lower sensitivity than the TES and the TES would become oversaturated if the same power at the photodiode was also directed to the TES, the power of the laser beam in the line of the TES must be attenuated. A variable attenuator is used for this purpose.
The task of this bachelor thesis is to determine the attenuation factor of the variable attenuator, whereby a maximum attenuation of $\approx$ -34 dB was achieved.

**Kurzzusammenfassung**

Diese Bachelorarbeit beschreibt die Charakterisierung der optischen Komponenten zur Bestimmung der Effizienz des Any Light Particle Search II TES-Detektors.
Diese Bachelor Arbeit wird im Rahmen des (ALPS II) Experiment, welches sich auf dem Gelände des Forschungszentrum des Deutsches Elektronen-Synchrotron (DESY) befindet, durchgeführt und geschrieben.
Das ALPS II Experiment soll schwach wechselwirkend Teilchen, den so genannten weakly interacting sub-eV particles (WISP) und somit zum Beispiel die Existenz von Axionen nachweisen. Diese Teilchen gelten als mögliche Kandidaten für die Dunkle Materie.
Um die Axione zu detektieren, wird ein Laserstrahl durch ein Magnetfeld geschickt, wobei die Photonen sich in Axione umwandeln könne. Eine Wand blockiert die nicht umgewandelten Photonen, mit der die Axione jedoch nicht wechselwirken. Die Axione werden dann in ein zweites Magnetfeld überführt und dort wieder in Photonen umgewandelt. Diese umgewandelten Photonen werden von einem Transition Edge Sensor (TES) gemessen. Da die erwarte Rate der umgewandelten Axione sehr niedrig ist, müssen die Verluste im TES ermittelt werden.

Dazu wird ein experimenteller Versuchsaufbau genutzt, bei der ein Laserstrahl, mit der selben Wellenlänge wie die der erwarteten Photonen, mit einem Strahlenteiler zum Tes und einer Photodiode zur Referenz Messung der Leistung geleitet wird. Da die Fotodiode eine niedrigere Empfindlichkeit hat als der TES und der TES bei gleichbleibender Leistung übersättigt werden würde, muss die Leistung des Laserstrahls gedämpft werden. Dafür wird ein variabler Attenuator verwendet.
Die Aufgabenstellung dieser Bachelor Arbeit ist den Dämpfungsfaktor des variablen Attenuator zu ermitteln. Wobei wurde eine maximale Dämpfung von $\approx$ -34 dB erreicht wurde.

# 1 Introduction

## 1.1 From the motion of stars to dark matter and what it is made of

Physicists have always been searching for the building blocks that make up our universe. In the process, they have come across astonishing results and have developed the standard model of modern physics that contains most of the building blocks of our matter.

Looking at the stars has also always aroused people's curiosity and raised many questions. One of these questions has been about the immediate environment of our planet. With the discovery of our neighboring planets, and thus the solar system, the gaze was directed to the nearest stars. These stars seemed to distribute themselves in spite of unimaginable distances after certain regularities and formed in their totality clusters, which were called Milky Way or galaxy. This Galaxy seemed to have a center around which all stars move on circular orbits.

If the total mass of all stars, gas and other more exotic objects, like black holes or other stellar corpses, was added together and it was assumed that the largest mass is concentrated in the center, the further the objects are away from the center, the lower the rotation speed should be. The rotation speed of objects in a galaxy are typically shown in "rotation curves," such as the one in Figure 1 below. One method of determining this is to measure the 21cm line of a neutral hydrogen atom with a radio telescope. However, astronomers concluded that the rotational velocity does not decrease with increasing distance.

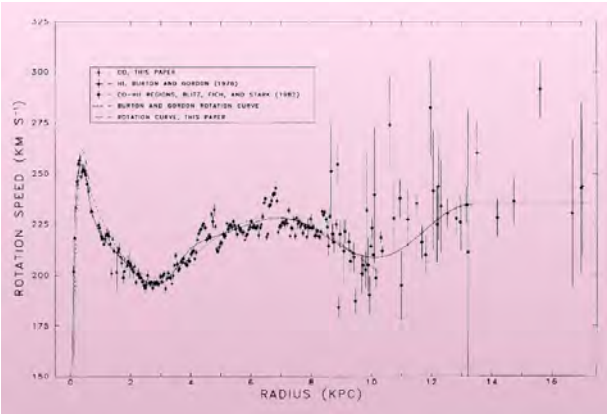


Figure 1: Here, the expected rotation velocity of the Milky Way's baryonic matter is plotted against the radius of the distance to the galactic center. It is compared with the observed total rotation velocity. Baryonic matter is the so-called "luminous matter" that interacts with electromagnetic radiation and, according to the current standard model of matter, consists of quarks and leptons. Rotational velocity is expected to decrease with increasing distance from the galactic center. However, it is observed that the rotaion curve has an almost constant velocity from a distance of about 4 kpc (13046.3 light years). From the different progressions curves it can be concluded that the total mass cannot consist exclusively of baryonic matter, but from another matter form, which is called dark matter [1].

After these observations, physicists were convinced that there must be an unknown matter in the Milky Way that does not interact with electromagnetic radiation and has only one mass. The so-called dark matter [2]. This anomaly of rotational velocities has also be observed in other galaxies.

Another indication of dark matter is gravitational lensing observed with telescopes. In this case, a large mass bends space to such an extent that the light is focused as in the case of a lens (see figure 2).

Figure 2: Here the galaxy cluster SMACS J0723.3-7327 can be seen with a large number of lensed background galaxies. The white bar at the bottom is approximately the maximum size of Jupiter (about 50 arcseconds) [3].

In this case, the mass of the observed luminous matter is not sufficient to explain the curvature of space. The gravitational lens effect can be explained only to the presence of further matter [4]. Since this is not observable, the assumption is obvious that it must concern dark matter which bends the space in such a way.

The scientific world was now faced with a great puzzle and various theories were put forward to identify dark matter and integrate it into the standard model.

The Standard Model of particle physics (SM) includes all particles known to modern physics [5]. It includes all elementary particles, the fermions, which include leptons and quarks, and the interaction particles, the bosons, as well as the Higgs particle, which was found only recently [6].

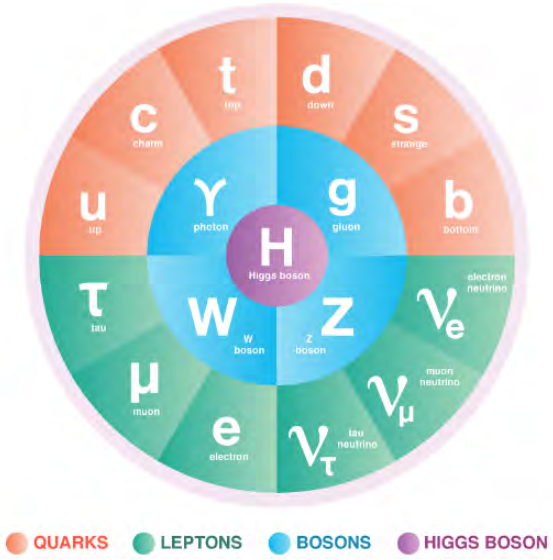


Figure 3: The standard model of particle physics describes all elementary particles known to modern physics. It is divided into 2 main groups, the fermions and the bosons. The fermions are divided into leptons and quarks and form the main component of our known matter. The bosons are interaction particles, which mediate the forces [7]

By embedding the Standard Model in theories such as supersymmetry, there is a theory from high-energy physics stating that it could be particles with weak interactions that have more than the mass of a proton or neutron. ($M_{WIMPs} > 1,67 - 10^{-27}kg$). The so-called weakly interacting massive particles (WIMPs). However, it has not yet been possible to detect these particles [8].

Another possible theory would be weakly interacting sub eV particles (WISPs) or axion-like particles (ALPs) [9]. These hypothetical particles would have a weak interaction with the particles of the Standard Model. They would have spin 0, would have no electric charge, and would have a low mass that could range from $8.91 \cdot 10^{-41}kg$ to $2.67 \cdot 10^{-39}kg$ [10]. The low mass would be compensated by their high number, so that they would have a multiple of the mass of the baryonic matter. The Axion would go beyond the standard model. However, it can effectively couple with two photons $\gamma$ via a pion $\pi$, as you can see in figure 4.

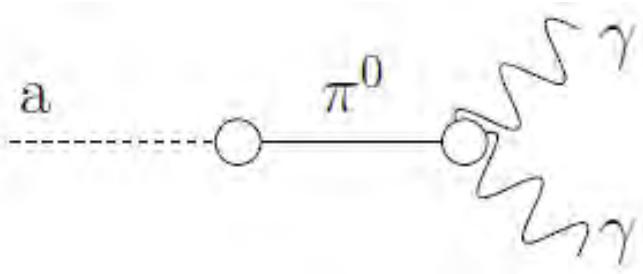


Figure 4: Coupling of an axion $a$ with a pion $\pi$ to two photons $\gamma$ [11].

The axion can transform into a photon under interaction of an external electrical and magnetic field and vice versa. This Primakoff-type interaction is called the Sikivie process, as you can see in figure 5 [12].

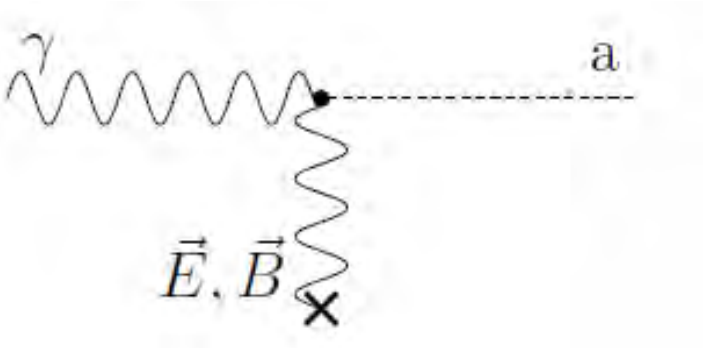


Figure 5: To and back conversion of an axion into a photon. This effect is called Sikivie effect [11] [12].

Due to the weak interaction of the axion with matter, the axion can pass through barriers that would stop a photon, as you can see in figure 6 [9]. This effect can be used for the detection of axions in so-called "Light Shining Through Walls" experiments [13] [14] [12].

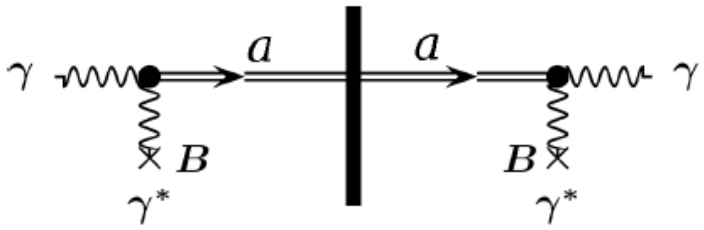


Figure 6: Photons are converted into axions in the magnetic field and can pass through the barrier. Photons are converted into axions in the magnetic field and can pass the barrier. On the other side of the barrier, the axions are converted back into photons in the magnetic field, which are detectable. [11].

The Axion was named by the Nobel Prize winner Frank Anthony Wilczek after the detergent Axion, because it would wash away the strong CP problem.

Motivation for the existence of the WISPs or axions is provided by the strong CP problem. In quantum chromodynamics, CP violationis understood as a violation of charge conjugation (C) and parity (P). P-invariance is the assumption that all physical laws must be the same after a mirror transformation. Charge conjugation invariance is the assumption that all interactions and decays of antiparticles are equivalent to their associated particles, i.e., C invariant. For example, the Coulomb force is invariant under charge conjugation. An example of the in the weak force CP violation is the charge and parity violation in the kaon. Kaons are hadrons subject to the strong interaction and thus are bosons. They belong to the meson family and consist of four different elementary particle combinations. They can become a $K^0$ or $K^+$ from an up quark u or down quark d each with an anti strange quark $\bar{s}$, or an anti up quark $\bar{u}$ an anti down quark $\bar{d}$ with

a strange quark s to a $K^-$ or $K^{-0}$. In 1964, the $K_L^0$ was found to be able to decay with a small probability to pions $\pi$. The problem is that the CP eigenstates exist in 2 different possibilities:

$$|K_S^0\rangle = \frac{1}{\sqrt{1+|\epsilon|^2}}(|K_1^0\rangle + \epsilon|K_2^0\rangle) \tag{1.1.1}$$

$$|K_L^0\rangle = \frac{1}{\sqrt{1+|\epsilon|^2}}(\epsilon|K_1^0\rangle + |K_2^0\rangle) \tag{1.1.2}$$

Where $\epsilon$ is the small difference between the eigenstates. This is an indirect but unambiguous CP violation.

In the Strong Force, such a CP violation is also expected, but has never been observed, even though it is not forbidden. The solution to the strong CP problem was proposed by Helen Quinn and Robert Peccei, which introduced a new spontaneously broken symmetry. Due to the broken symmetry, a new particle should be created, which was called axion. The axion is then the solution to the strong CP problem [15] [16]. And the axion is also a candidate for the cold dark matter [17].

One way to detect axions is the Any Light Particle Search II (ALPS II), in which light passes through a strong magnetic field to convert photons into axions, which then pass through a wall and are converted back into photons by another magnetic field on the other side of the wall [6].

## 1.2 ALPS II Experiment


Figure 7: Photo of a part of the ALPS II Experiment [18]

In the ALPS-II experiment as can be seen in the photo 7 and in the sketch 8, a 30 W [19] laser beam with a wavelength of 1064 nm is directed into an optical cavity where it is amplified to a power of 150 kW [20].

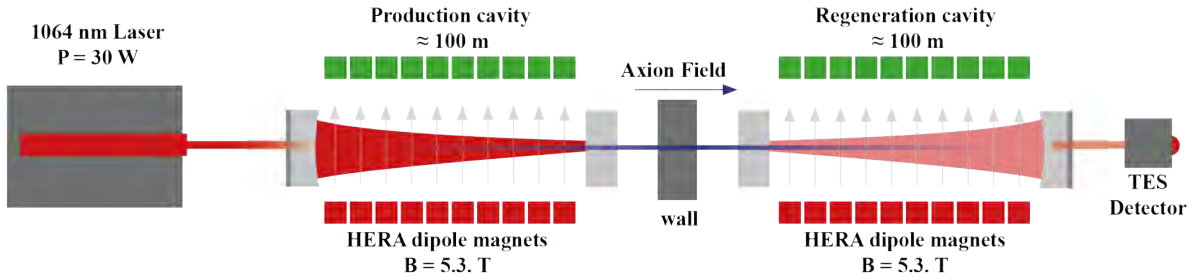


Figure 8: Sketch of the setup up of the ALPS II experiment. The laser is immersed in a magnetic field and there the photons convert in axions. The photons are blocked by a wall with which the axions do not interact. The axions can them propagate though to another magnetic field where they are converted back into a photon which is then detected by the TES detector [20].

In the optical cavity there is a HERA dipole magnetic chain with 5.3 T [19]. Theoretically, axion-like particles should arise from photons in the magnetic field, which have a very small mass ($m_{axion} \ll m_{electron}$) [21], due to the Sikivie effect explained in section 1. These axions are also called weakly interacting sub-eV particles (WISP) [22]. The resulting axion can then penetrate a wall at which the photons are blocked. Behind the wall, the axion returns to an optical cavity with dipole magnets, where the axion is converted back to a photon with an energy of about 1.16 eV [19] and can be measured by the Transition Edge Sensor. Blocking the photons in the first part of the experiment ensures that no photon from the laser beam can reach the TES and thus only the light induced by an axion can be measured.

The expected photon power and the expected photon rate are calculated by the following equation 1.2.2 and 1.2.1:

$$R_{exp.,photon} = 2\frac{photons}{day} = 2.31 \cdot 10^{-5}\frac{photons}{second} \tag{1.2.1}$$

$$W_{photon} = R_{exp.,axion} \cdot 1eV = R_{exp.,photon} \cdot 1.60218 \cdot 10^{-19}J = 3.701 \cdot 10^{-24}\frac{J}{s} \tag{1.2.2}$$

Where $R_{exp.,axion}$ is the expected photons rate from the axion and $W_{photon}$ the expected power of the photon.

The TES is one of two detectors designed to detect axions first converted from photons to axions and then re-converted to photons.

## 1.3 Transition Edge Sensor (TES)


(a) The cryostat in the assembled state, which is installed in this state after the test phase in the ALPS 2.

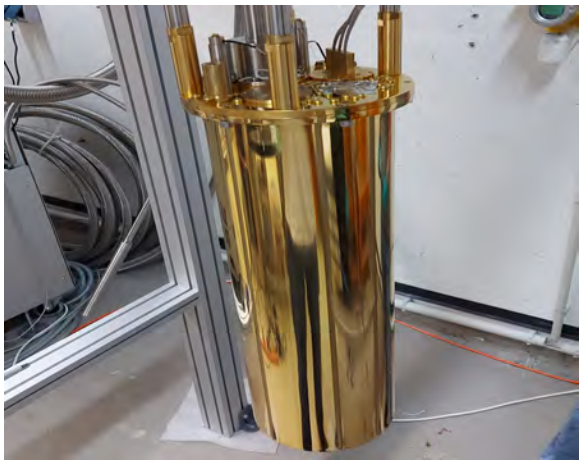

(b) The cryostat in disassembled state, with only the intermediate stages of cooling.

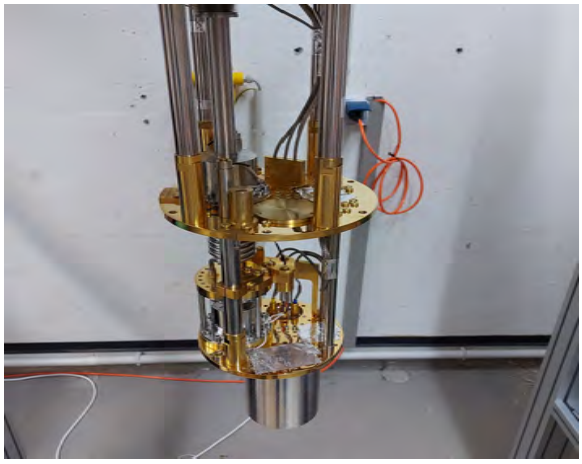

(c) The cryostat in a further disassembled state, with the TES sitting at the bottom in the silver cylinder.

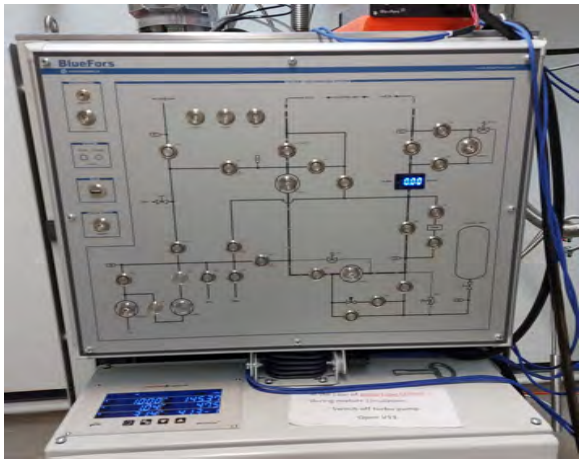


(d) The control station of the cryostat, which is responsible for cooling the TES.

Figure 9: Here you can see the cryostat. The TES is inside this cryostat and is cooled down so that the sensor reaches a near superconducting state.

At the planned sensitivity, we expect 1-2 converted photons per day. To detect such a low photon rate, we need a sensitive detector, a Transition Edge Sensor (TES). The TES is made of tungsten that it is between the transition of superconducting and conducting. In this state, a photon would have the necessary energy to heat the current-carrying material and move it from the transition from superconducting, (by cooling the tungsten to 140 mk), to normal conducting, as can be seen in Figure 10.

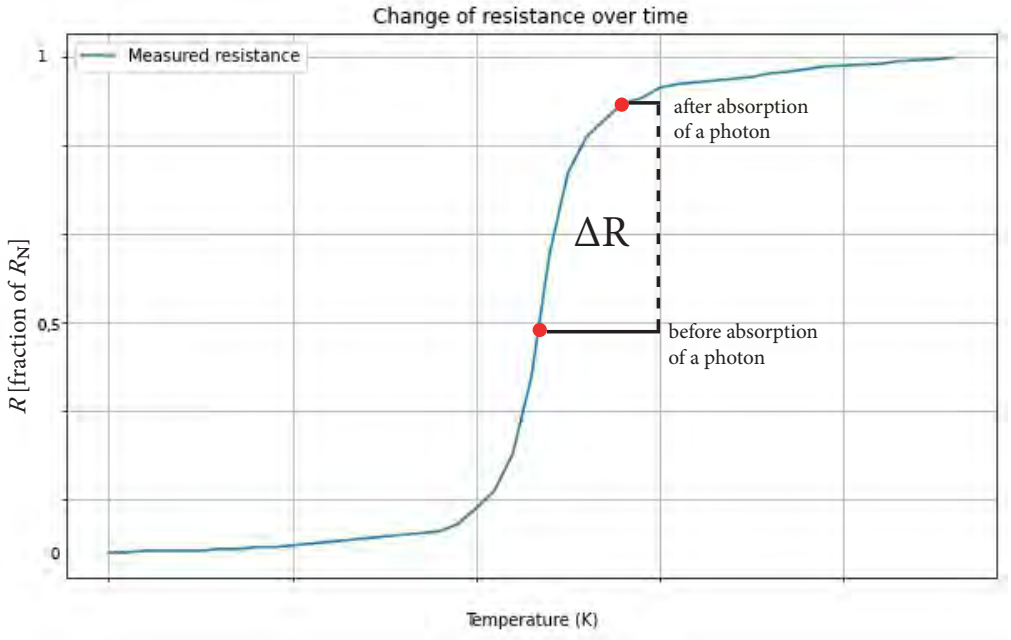


Figure 10: This is a sketch to illustrate the operation of measuring a photon. A piece of tungsten (25um x 25 um x 20 um), is in a state between superconducting and normal conducting to ensure high sensitivity. By receiving a photon, the temperature of the tungsten increases and this is sufficient to bring the intermediate state of the material to the conducting state. Since the piece of tungsten is under a permanent voltage, the resistance changes. The change in resistance results in a change in current, which is measured by the SQUID electronics. This makes it possible to measure low energy photon beams.

In the process, an increase in resistance becomes measurable. In this way, extremely high sensitivity can be achieved. The TES is cooled with a dilution refrigeration cryostat (see figure 9). The material is connected to a constant current source. When incident photons are absorbed by the material, is absorbed by the material, it heats up and changes the resistance of the material, which causes a change in current that is registered using SQUID electronics as a change in voltage over time. We can determine the energy of the incident photon from the integral of this voltage pulse. The photon we are looking for has the energy 1.165 eV [22]. Another effect of the cooling is the shielding of blackbody radiation, which emanates from all warm bodies that have a temperature above 0 K and are strongly temperature-dependent. The blackbody radiation that couples into the optical fibers when warm can propagate through the cryostat via the fibers and impinge on the TES, resulting in increased background and thus distorting the measurements. Besides blackbody radiation, cosmic rays and radioactivity also interfere with measurements in the TES by causing unwanted backgrounds.
To counteract the backgrounds from Blackbody radiation, a wavelength filter is placed in front of the TES, as you can see in the sketch of the TES 11). This filter is realized by fiber curling and filters to only allow wavelengths $< 1550nm$.

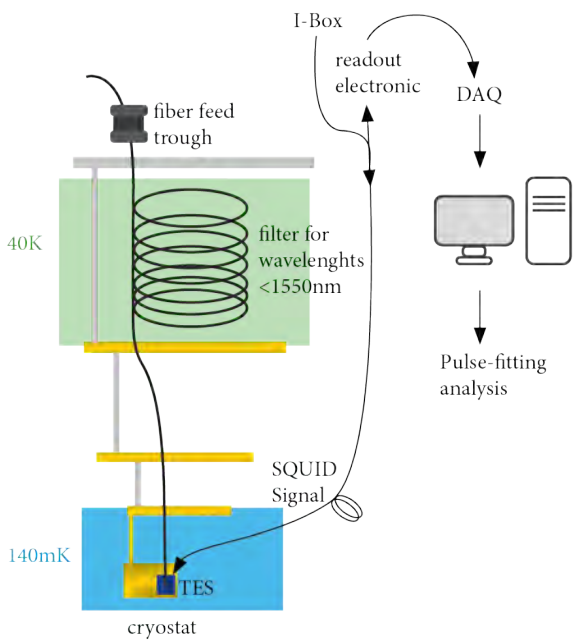


Figure 11: TES detector sketch

A superconducting quantum interference device (SQUID) , as you see in sketch 11, is used as a readout for signals in the TES, which can measure the current changed by the measurement of the photon in the TES with very low noise. This is a sensitive magnetic flux sensor that detects the magnetic flux through the SQUID loop into a voltage or current. The received data is then analyzed and interpreted with the aid of a computer program.

## 1.4 Determine the efficiency of the Transition Edge Sensor (TES) for 1064-nm photons, to verify the losses in the TES

The efficiency of the TES for 1064-nm photons is to be determined in order to check how strong the losses in the TES system are. For calibration, a 1064-nm laser is used, which is split into 2 beams via a beam splitter, as can be seen in the figure 12. The first beam runs as a reference measurement into a calibrated photodiode (calPD), for which there is a known conversion between the output voltage of the photodiode and the corresponding power. The second beam is directed into the TES. To avoid oversaturation of the photodiode, the total power of the laser is attenuated by a Schäfter Kirchhoff (SK) attenuator block positioned directly behind the laser and before the beam splitter.

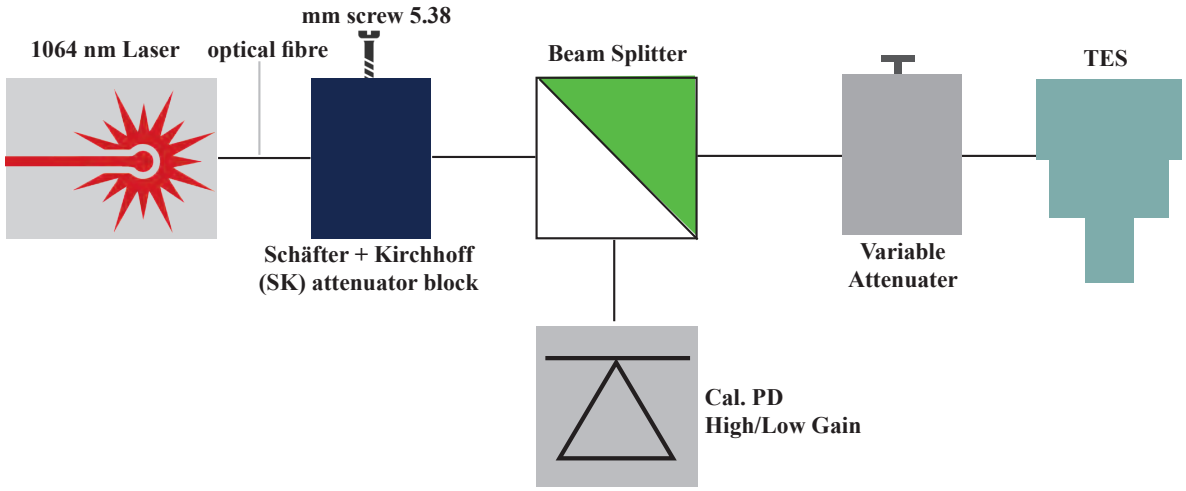


Figure 12: Sketch of the setup to determine the efficiency of the Transition Edge Sensor (TES) for 1064-nm photons, to check the losses in the TES.

Since the power of the laser is too high for the efficiency measurement, an additional variable attenuator specifically suited for 1064 nm is used. For this purpose, its attenuation factor must be determined in order to then determine the actual power that was sent to the TES, with reference to what was measured with the calPD. The calibration of the variable attenuator is done by a further setup, which is described in the section Experimental Setup (section 3) and its realization in the section Procedure to determine the attenuation factor: a step-by-step guide, see section 4.2.1.

## 1.5 Determination of the efficiency of the TES

To determine the efficiency $\epsilon$ of the TES, as described in section Determine the efficiency of the Transition Edge Sensor (TES) for 1064-nm photons, to verify the losses in the TES (section 1.4), in figure 12 the following equation 1.5.1 must be used:

$$\epsilon = \frac{P_{TES}}{P_{in}} \tag{1.5.1}$$

Wherein $P_{TES}$ is the Power that reaches the TES and $P_{in}$, the Power irradiated into the experimental setup

The irradiated power $P_{in}$ is calculated 1.5.2 with the Power measured by the photodiode $P_{PD}$, the Maximum damping of the variable attenuator $L_p$ and $r$. Wherein $r$ is the splitting from the beam splitter, see Experimental test setup section 3. Here $r$ is the $99\%$ line and $1 - r$ is the $1\%$ line.

$$P_{\text{in}} = \frac{1-r}{r} P_0 \times 10^{L_P/10} \tag{1.5.2}$$

The maximum attenuation of the variable attenuator $L_P$ is determined in the experiment. With the following equation 1.5.3 an approximate ideal value for the attenuation can be determined based on the maximum power that the TES can handle.

$$L_P = 10 \log_{10} \left( \frac{r}{1-r} \frac{hc}{\lambda} \frac{n_{\text{TES}}}{\epsilon P_{0\,\text{min}}} \right) \tag{1.5.3}$$

The power measured by the TES $P_{TES}$ is determined with the Planck´s constant $h$, the speed of light $c$, the detected photon rate of the TES $n_{TES}$ and $\lambda$, which is $1064nm$, by the following equation 1.5.4:

$$P_{TES} = \frac{hc}{\lambda} n_{TES} \tag{1.5.4}$$

To be able to calculate the ”true” number of photons $\mu$ hitting the TES, the Poissen distribution **??** for lasers can be used. Where $N$ is the number of all photons.

$$p_n = e^{-\mu} \frac{\mu^N}{N!} \tag{1.5.5}$$

The Poissen distribution 1.5.5 must now be solved for $\mu$ by logarithmizing the equation. The resulting constant $C$ can be neglected.

$$\ln(p_n) = -\mu + N \cdot \ln(\mu) + C \tag{1.5.6}$$

In order to determine the "true" number of photons $\mu$, the derivative of the probability to detect a photon $p_n$ is formed and set equal to zero to find the maximum.

$$\frac{d\ln(p_n)}{d\mu} = -1 + \frac{N}{\mu} = 0 \tag{1.5.7}$$

The equation for $\ln(p_n)$ becomes zero when $N = \mu$.

With the maximum rate we can process at the TES ($n_{\mathrm{TES}} \lesssim 4.5 \cdot 10^3 Hz$ [1]) to use Eq. 1.5.3 and 1.5.4 to estimate the required attenuation $L_p$. See Sec. 1.1 of the document [23].

[1] That measurement was done to characterize the TES response for different working points (WPs) and different gain width products (GBWPs). We use the measurement taken over 1 s with with WP set to $0.3\,R_N$ and GBWP set to 1.5 GHz. The input file is available here:
`/data_local/backup_WorkingPointData/WorkingPointData/WorkingPointLightData` on `alpsdaq2`.

# 2 Task of the bachelor thesis

**The task is to determine the possible attenuation of the 1064 nm laser power in dB of the attenuator.**

In order to determine the efficiency of the TES system, a variable attenuator is needed, which attenuates the power of the laser to the beam and which is positioned in front of the TES (see section 1.4). This is because the photodiode used for the reference measurement is not as sensitive as the TES and thus requires a higher power compared to the TES. However, the TES itself would be damaged at this power. Therefore the attenuation of the attenuator has to be measured first to make the reference measurement comparable to the measurement of the TES. For this purpose, another experimental setup is needed, see section 3.

It should also be checked whether the light shining in the laboratory has an influence on the measurement. For this purpose, a series of measurements is made with the light switched on and another series of measurements with the light switched off.

Another part of the task is to create a step-by-step guide that explains the measurement of attenuator damping effectiveness.

# 3 Experimental setup for measuring attenuation

In the experimental setup, a 1064-nm laser with optical fibers is connected to an attenuator block, which can be used to control the input laser power of the setup. The output of the Schäfter Kirchoff (SK) attenuator block leads to a beam splitter that divides the laser beam into two parts, with one part having 99% of the power and the other part having 1% of the power. The 99% line is used to calibrate the variable attenuator, which is used to determine the TES efficiency. The 1% line is not used further in this process. The 99% line is connected to the variable attenuator through a fiber connector (FC), and its output is connected to a calibrated photodiode (calPD). The calPD is in turn connected to the grid-connected FPGA-based test and measurement board called RedPitaya. Via the RedPitaya, the measurement data of the photodiode in volts are forwarded to a computer terminal, where they are stored.

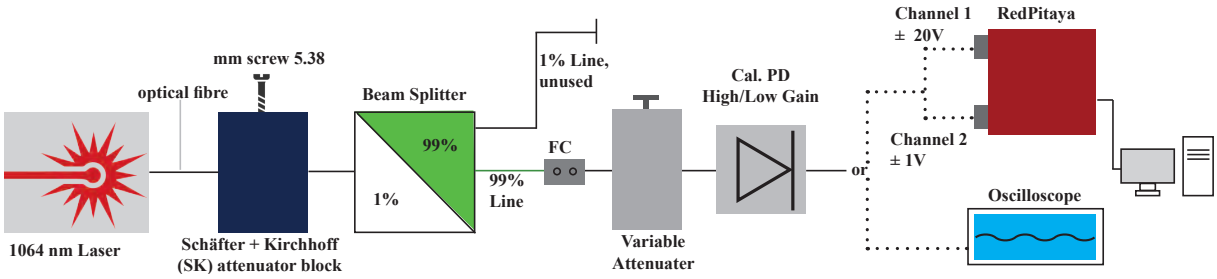


Figure 13: Sketch of the experimental setup for determining the attenuation. The power of the laser is reduced by the variable attenuator and then measured with the photodiode and the Red Pitaya.

First, the noise of the experimental setup is to be determined with the laser switched off. For this purpose, 4 measurements are made with a photodiode and a RedPitaya, channel 1 of the RedPitaya with a range of $\pm 20$ V, high and low gain, and channel 2 with a range of $\pm 1$ V, high and low gain for 10 minutes, with the SK Attenuator Block and the Variable Attenuator fully open.

Then with the laser turned on and the variable attenuator fully open (minimum attenuation), the SK Attenuator Block is adjusted so that the maximum power at the calPD is reached, without saturating the device. The calPD saturates at 12 V, so close the attenuator cube to the point where it is as close to 12 V as possible, without fully reaching 12 V (eg 11.8 V). This should be done using an oscilloscope and watching the output voltage as the knob is opened/closed. From this point on, the Attenuator Block should not be adjusted any further. At the point where saturation occurs (11.8 V), the power $P_0$ is measured, which is later used as a reference value in the equation 4.1.3.

Then, with the laser on, make 5 more measurements, increasing the attenuation of the attenuator with each measurement so that the laser power decreases until 1V is reached. For these measurements from about 12 V to 1 V, use channel 1 $\pm$20 V and low gain to minimize noise. The final measurements are made at an attenuation where the photodiode has reached the limits of sensitivity. This is done below 1 V, using Channel 2, $\pm$ 1 V, and high gain. The data is then plotted over time, and the standard deviation and average, as well as the power and attenuation, are calculated and plotted on a graph.

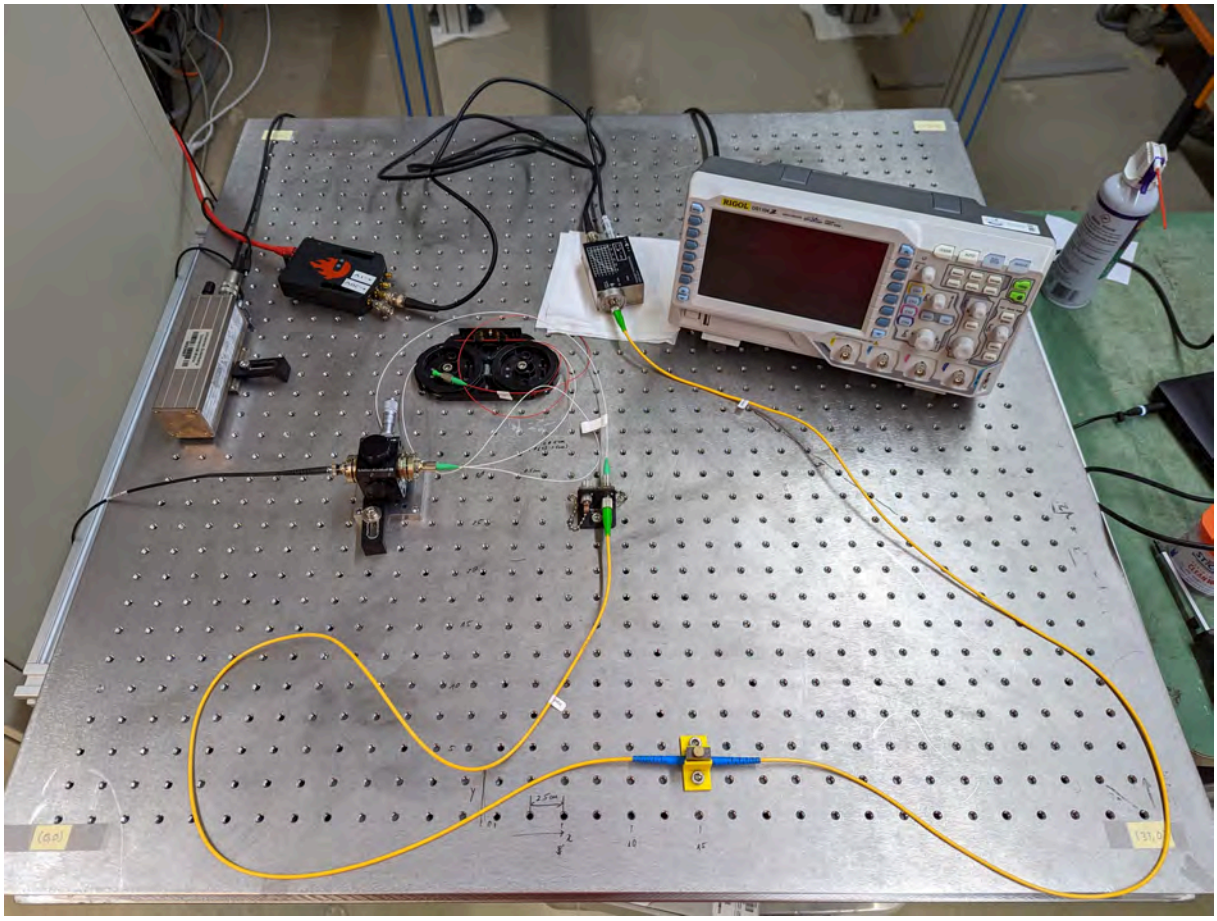

Figure 14: Photo of the experimental setup to determine the attenuation of the variable attenuator.

# 4 Results

This section describes the measurement results, as well as their interpretation.

## 4.1 Measurement results of the measured power and calculated attenuation

In the following, the measured values of the attenuation of the variable attenuator are measured in volts. The noise in volts was then subtracted from these values in volts according to the following equation 4.1.1.

$$\langle V_{\mathrm{true},i,g} \rangle = \langle V_{\mathrm{meas.},i,g} \rangle - \langle V_{\mathrm{Noise},i,g} \rangle \tag{4.1.1}$$

$\langle V_{\mathrm{true},i,g} \rangle$ = Mean value of the true voltage value after noise subtraction
$\langle V_{\mathrm{meas.},i,g} \rangle$ = Mean value of the measured voltage with damped power and laser switched on
$\langle V_{\mathrm{Noise},i,g} \rangle$ = Mean value of the measured voltage with the laser switched off

Then the voltage will be converted to the power of the laser, which is done in the equation below [4.1.2]. Voltage-to-power conversion at low and high gain are taken from Fig. 15 of ref. [24] which has been determined by the Physikalisch-Technische Bundesanstalt (PTB).

$$P = \begin{cases} \frac{\langle V_{\mathrm{true},i,g} \rangle + 0.0012}{5.865 \times 10^8}, & g = \text{low gain} \\ \frac{\langle V_{\mathrm{true},i,g} \rangle - 0.0057}{5.837 \times 10^9}, & g = \text{high gain} \end{cases} \tag{4.1.2}$$

Where $P$ is the measured power of the Laser (attenuated or unattenuated power)

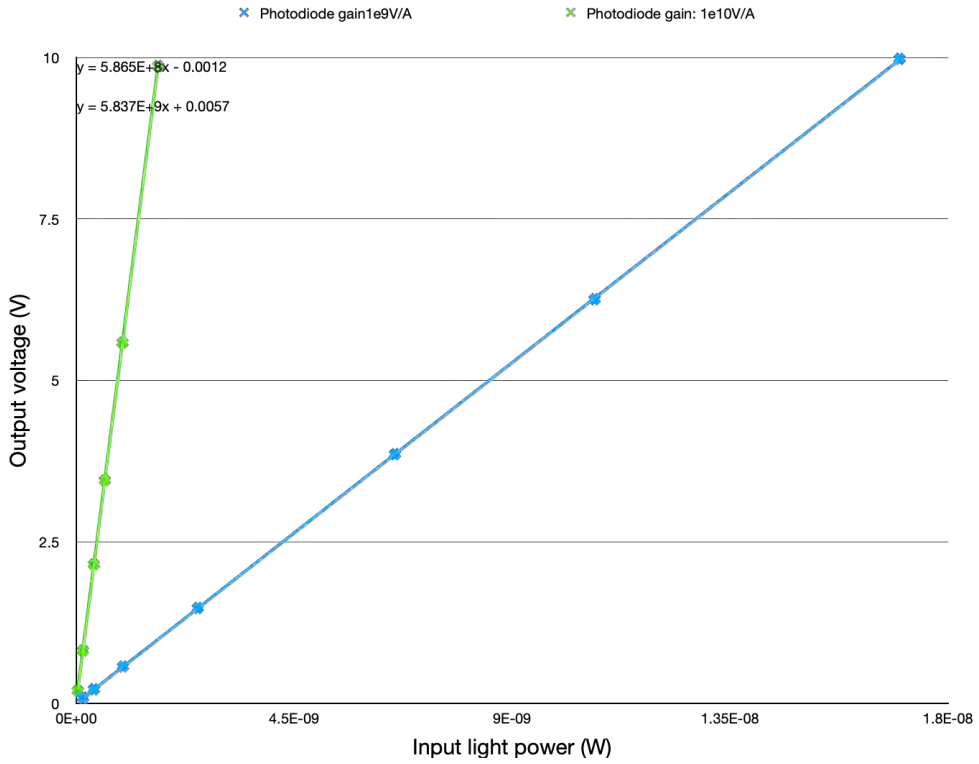


Figure 15: Behaviour between input power and output voltage of the calPD [24]

The calculated power is converted to the attenuation $L_p$ [dB] in each case, where the power of the current attenuated measurement $P_{\text{w/ atten}}$, refers to the power without attenuation $P_{\text{w/o atten}}$, which was detected during the first measurement. The following equation is used for this purpose.

$$L_P = 10 \log_{10} \left( \frac{P_{\text{w/ atten}}}{P_{\text{w/o atten}}} \right). \tag{4.1.3}$$

To calculate the error, first calculate the standard deviation of the voltage and power with $\sigma_{voltage,power}$ of the measurement of the voltage, as well as the power. Gaussian errors are assumed to be present.

$$\sigma_{voltage,power} = \sqrt{\frac{1}{n-1} \sum_{i=1}^{n} (x_{i(voltage,power)} - \bar{x}_{(voltage,power)})^2} \tag{4.1.4}$$

Where $x_{i(voltage,power)}$ is the measured values of the voltage or the converted power for each measured value and $\bar{x}_{(voltage,power)}$ is the mean value of the measured values of the voltage or the converted power for each measured value. The results of $\sigma_{voltage,power}$ are shown in the table 2 and in table 1.

The uncertainty in the calculation of the attenuation $\sigma_{xi}$ is calculated by the standard deviation $\sigma_{yi}$ of the power with or without attenuation plus the standard deviation $\sigma_{zi}$ of the power of the relevant noise, using the following equation.

$$\sigma_{xi} = \sqrt{\sigma_{yi}^2 + \sigma_{zi}^2} \tag{4.1.5}$$

To calculate the error of the attenuation, an error propagation $\Delta L$ must be implemented. Where the $\sigma_{xi}$ is the respective uncertainty as calculated in equation 4.1.5.

$$\Delta L = \sqrt{\left( \frac{\mathrm{d}L_p}{\mathrm{d}P_{\text{w/ atten}}} \cdot \sigma_{xi} + \frac{\mathrm{d}L_p}{\mathrm{d}P_{\text{w/o atten}}} \cdot \sigma_{xi} \right)^2} \tag{4.1.6}$$

The results for $\Delta L$ are shown in the table 1.

### 4.1.1 The stability of the laser Test

The stability of the laser was first measured over a period of about 20 hours. The laser is connected to the experimental setup to determine the attenuation (see sketch 13), without one of the attenuators reducing the power. The measurement is performed in high gain and channel $1 \pm 20$V.

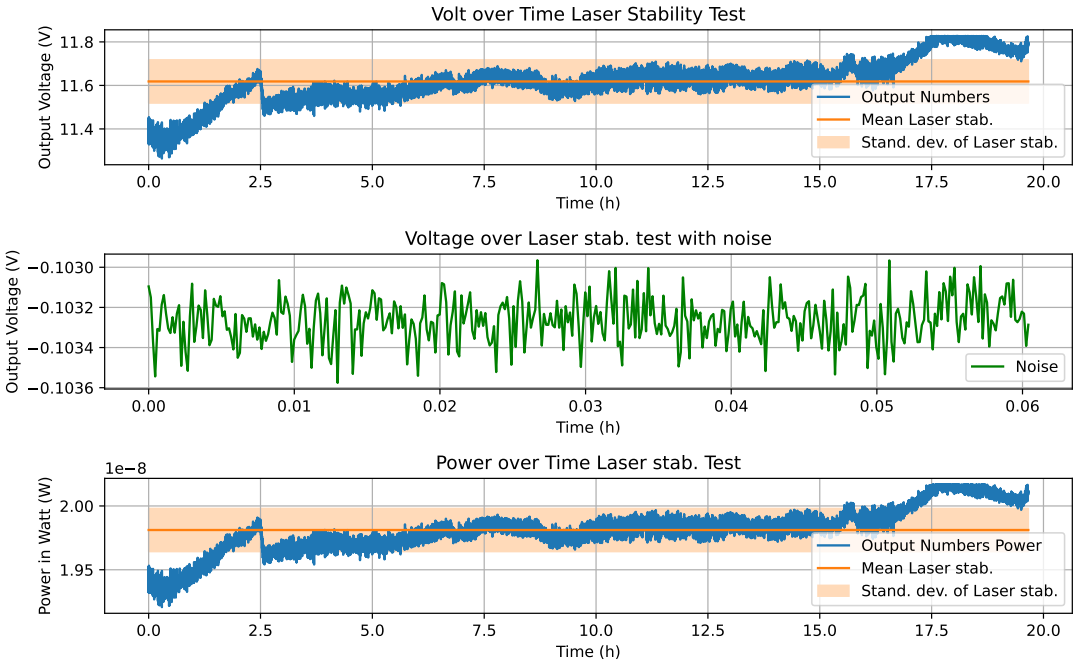


Figure 16: The measurement of the stability of the laser. The first plot shows the voltage over the time of about 20 hours. The second plot compares the voltage over time with the noise measured later. The third plot shows the voltage over time versus the converted power of the laser.

In figure 16 the measurement results of the laser stability in volts are plotted as a function of time with the mean and standard deviation in the first plot. The second plot shows the noise of the experimental setup (see sketch 13). Here the laser was switched off and only the noise was recorded. This is described in more detail in the section 4.1.2. The third plot shows the converted power with mean and standard deviation of the laser.
It can be clearly seen that the performance varies greatly in the first 3 hours. From hour 0 to approx. 2.5, the power is far below the mean value and slowly approaches the mean value. In the period around 2.5 hours, the power curve shows a rapid weakening. After that, the power stabilizes for about 13 hours and then increases again. From these results it can be concluded that the laser should be switched on at least approx. 3 hours before the actual measurement, so that a good stability of the laser can be achieved.

### 4.1.2 Determination of the dark noise of the entire experimental setup

The measurement of the noise of the experimental setup was performed by connecting all the components (see the experimental setup in section 3), but the two attenuators were fully opened and thus did not attenuate. Here, the photodiode was first connected to Channel 1 $\pm$ 20V in low and high gain and then to Channel 2 $\pm$ 1V in low and high gain so that the noise of both channels could be compared. The measurement was performed for about 10 minutes. The results are shown in figures 17, 18, 19, 20. The first plot shows the measured voltage values and the second plot shows the converted power.

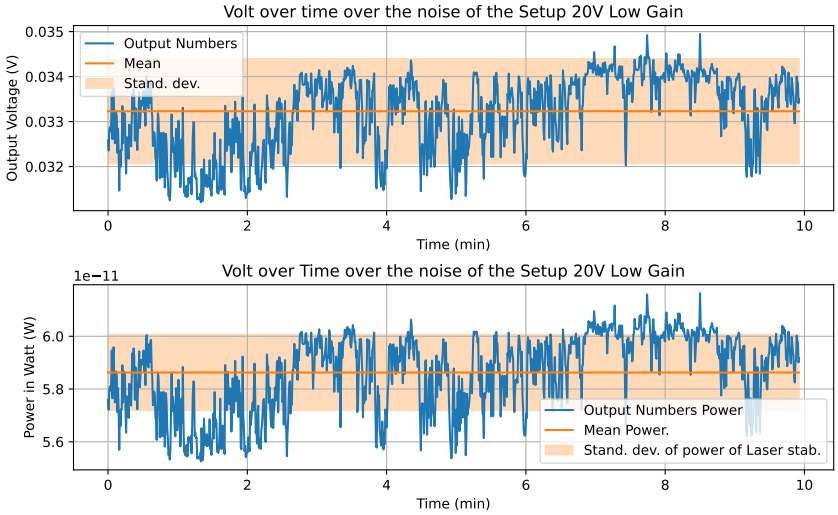


Figure 17: The noise in Channel 1 $\pm$ 20V in low gain

The noise in Channel 1 $\pm$ 20V in low gain is at a mean value of $0.030 \pm 0.002$ V or $58.6 \cdot 10^{-12} \pm 1.43 \cdot 10^{-12}$ W.

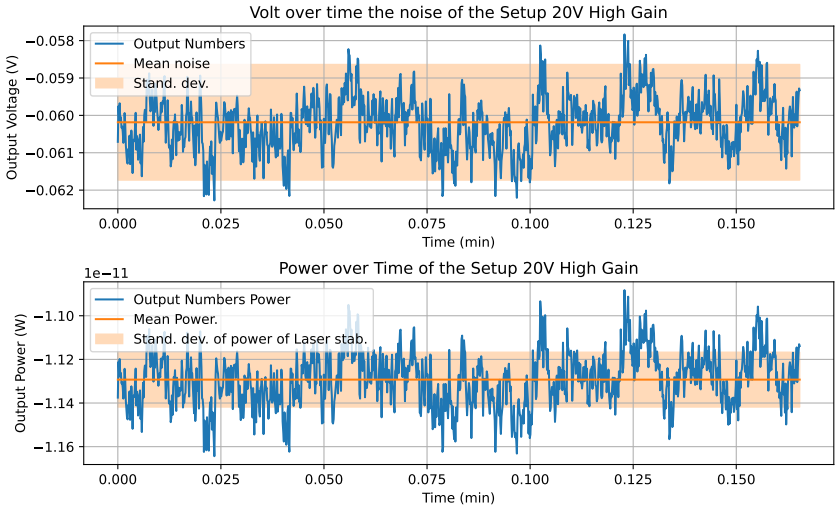


Figure 18: The noise in Channel 1 $\pm$ 20V in high gain

The noise in Channel 1 $\pm$ 20V in high gain is at a mean of $-0.060 \pm 0.002$ V or $-113.0 \cdot 10^{-13} \pm 1.26 \cdot 10^{-13}$ W.

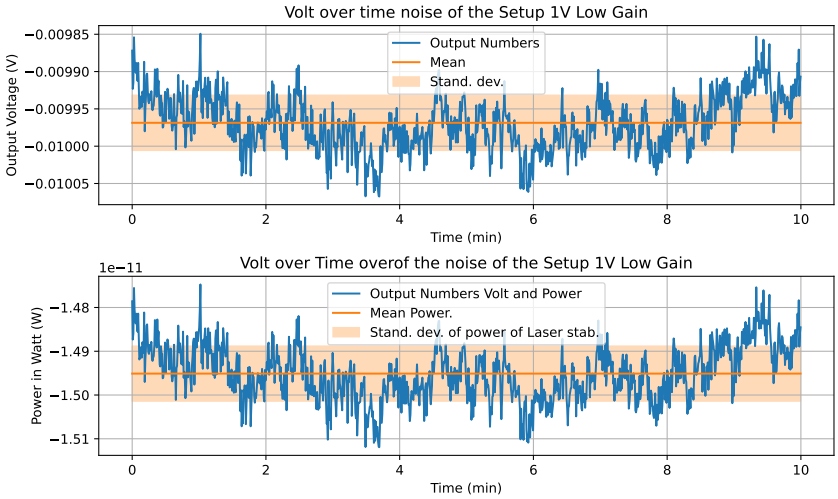


Figure 19: The noise in Channel 2 $\pm$ 1V in low gain

The noise in Channel 2 $\pm$ 1V in low gain is at a mean value of $-0.01 \pm 0.0004$ V or $-1.49 \cdot 10^{-11} \pm 6.29 \cdot 10^{-14}$ W.

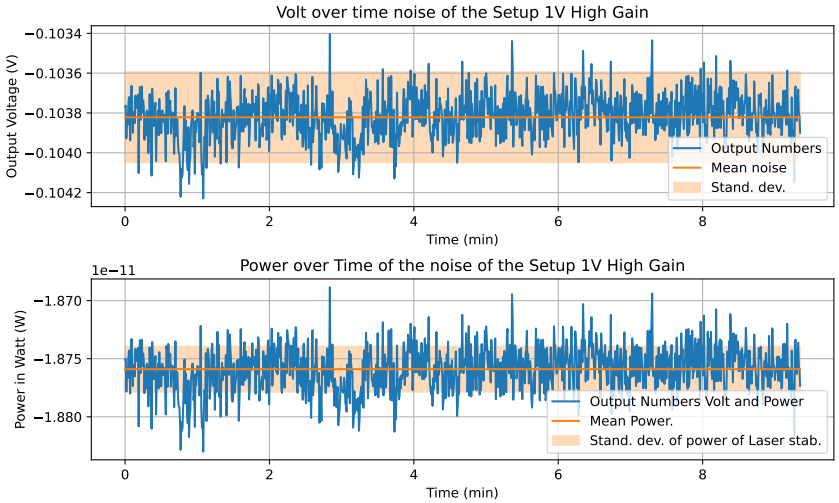


Figure 20: The noise in Channel 2 $\pm$ 1V in high gain

The noise in Channel 2 $\pm$ 1V in high gain is at a mean of $-0.10 \pm 0.0002$ V or $-1.88 \cdot 10^{-11} \pm 1.96 \cdot 10^{-14}$ W.

It can be observed that in Channel 1 $\pm$ 20V at high gain, as well as in Channel 2 $\pm$ 1V at

| Measurement | Voltage mean [V] | Power mean [W] |
|---|---|---|
| Channel 1 $\pm$ 20V low gain | $0.030 \pm 0.002$ | $5.86 \cdot 10^{-11} \pm 1.43 \cdot 10^{-12}$ |
| Channel 1 $\pm$ 20V high gain | $-0.060 \pm 0.002$ | $-1.13 \cdot 10^{-11} \pm 1.26 \cdot 10^{-13}$ |
| Channel 2 $\pm$ 1V low gain | $-0.01 \pm 0.0004$ | $-1.49 \cdot 10^{-11} \pm 6.29 \cdot 10^{-14}$ |
| Channel 2 $\pm$ 1V high gain | $-0.10 \pm 0.0002$ | $-1.88 \cdot 10^{-11} \pm 1.96 \cdot 10^{-14}$ |

Table 1: In this listing table the results, as well as the calculated values of the measurement series for the determination of the noise of the measurement setup are written down.

high and low gain the measured values are negative. These must then be introduced into the damped measurements, especially when determining the true value, so that they do not falsify the measurements by changing the sign when calculating the true value. When calculating the True Value, the noise is subtracted from the measured value. In the case of a negative value, it would be added. Therefore, the sign can be changed and thus the amount of noise can be subtracted from the measured value. Channel 1 $\pm$ 20V at low gain the values are however positive. This Channel and the gain are used for the first 5 measurements of the attenuation as reference value and for the determination of the true value. The values from the measurement of the noise of Channel 2 $\pm$ 1V at high gain are used in the last measurements (near the absolute limit of the sensitivity of the photodiode) as reference value and to calculate the true value.

### 4.1.3 Calculation of the expected power for blackbody radiation

To estimate the influence of the blackbody radiation (BB) on the experiment, the power per time can be calculated (Equations and values were taken from the following Confluence [2] page). For this purpose, the number of BB photons $N(E,T)$, which depend on the energy E and the time T, is calculated with the following equation 4.1.7:

$$N(E,T) = \frac{2E^2}{h^3c^2}\frac{1}{e^{\frac{E}{kT}}-1} \tag{4.1.7}$$

Where the maximum is at $E = xkT$ , with $x \approx 2.82$, $h$ is the planck constant, $c$ is the speed of light, and $k$ is the boltzmann constant. The number of BB photons $N(E,T)$ can now be multiplied by the energy and integrated over the energy 4.1.9. Integration over energy gives the energy flow per area per time. To obtain the energy per time, the integral must be multiplied by the area $A = 78.5\mu m = 7.85 \cdot 10^{-4}m$ and the solid angle $\Omega = 0.07sr$. Since the Expected Radiation is in a wavelength range of $\lambda = 500 - 2000nm$, this must still be converted to the energy in the equation 4.1.8 and can then be used as the limits of the integral.

$$E = \frac{hc}{\lambda} \tag{4.1.8}$$

With $2000nm = 2 \cdot 10^{-6}m$ and $500nm = 5 \cdot 10^{-7}m$, the limits of energy follow:
$E_{\lambda=2000} = 9.93237 \cdot 10^{-20}$
$E_{\lambda=500} = 3.97295 \cdot 10^{-7}$

From this follows the integral:

$$\int_{3.97\cdot10^{-7}}^{9.93\cdot10^{-20}} E * N(E,T)dEdAd\Omega = A \cdot \Omega \cdot \int_{3.97\cdot10^{-7}}^{9.93\cdot10^{-20}} \frac{2E^2}{h^3c^2}\frac{1}{e^{\frac{E}{kT}}-1}dE \tag{4.1.9}$$

The expected power for the blackbody radiation is $4.05 \cdot 10^{-17}\frac{J}{s}$.

[2] https://confluence.desy.de/display/ATES/Direct+Photon+contribution

### 4.1.4 Light pollution test

A test was made to see if the measured values change when the light in the laboratory is switched on and off, in order to determine other possible sources of interference and to exclude them if necessary. Each measurement was performed over 5 minutes.

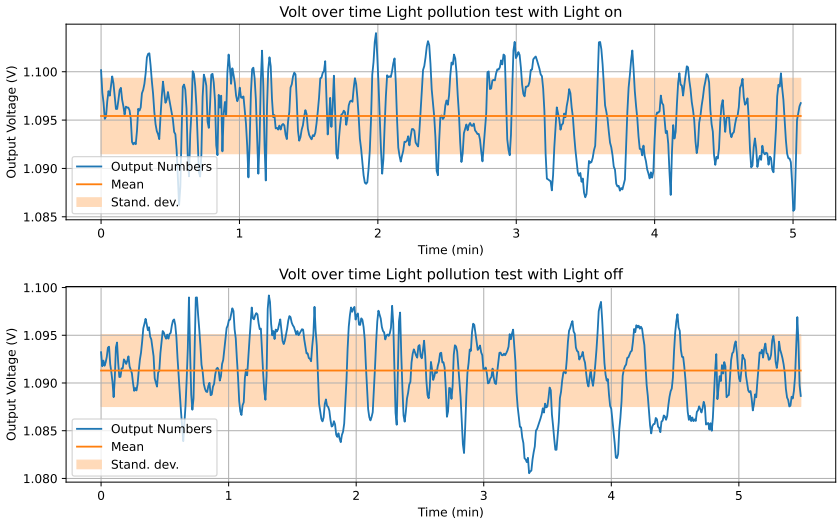


Figure 21: Measurement with the light switched on and off in the laboratory

In figure 21 it can be seen that the mean value of the measurement with the light on light at $1.095 \pm 0.004$V and with the light off light $1.091 \pm 0.004$ V. Here it can be seen that the light in the laboratory has no discernible influence on the measurements and can therefore be excluded as a source of error.

### 4.1.5 Measurements of the attenuation of the variable attenuator

The main measurement was to determine the attenuation capability of the variable attenuator. For this purpose, the threshold is sought above which the laser power at the calPD is maximized without bringing it into saturation. This is done by adjusting the SK attenuator block accordingly, as described in section 3. The later attenuation was then done with the variable attenuator. The measurements were made in 7 steps. The first measurement (see figure 22) was made without any attenuation and thus represents the reference value of the power to determine the attenuation in dB. In the intermediate measurements, the attenuation was increased in each measurement. The last measurement (see figure 23) represents the largest attenuation and is related to the first measurements, using the equation to calculate the absolute attenuation of the attenuator. Each measurement was performed over 10 minutes. The measured values were calculated with the noise so that the true value could be calculated. The values are given in the table 2. Measurement series 2 - 6 (to see from figure 25 to 28), showing the measurements with increasing attenuation, are attached in the appendix A.

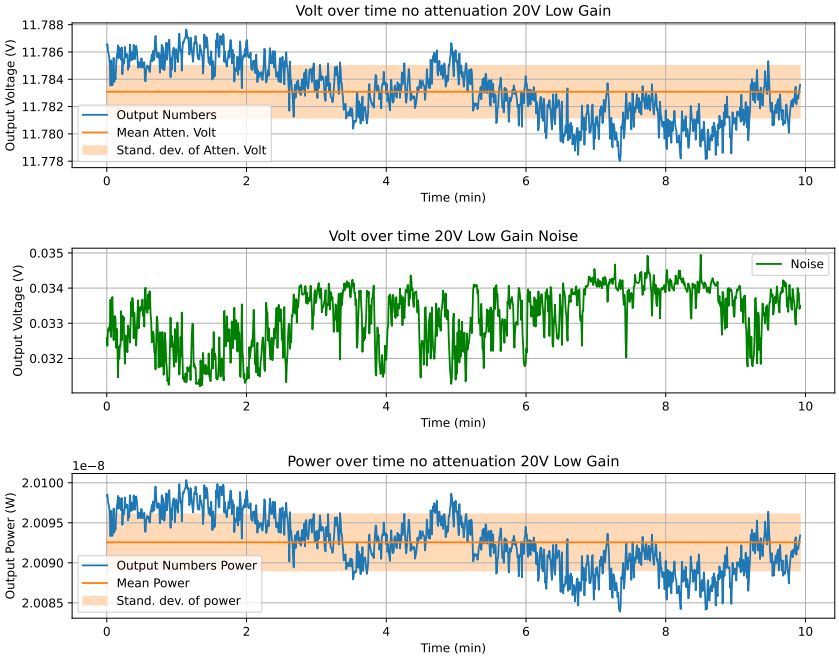


Figure 22: The first measurement of the attenuation of the variable attenuator whereby without damping. In the first plot, the voltage is plotted versus time. In the second plot, the voltage is compared to the noise and in the third plot, the voltage versus time is plotted versus the calculated power.

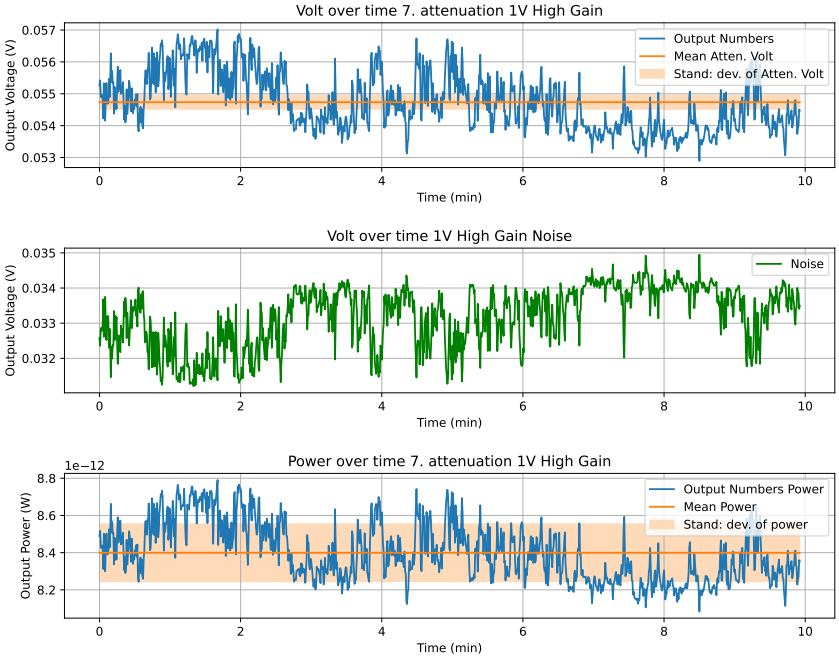


Figure 23: The seventh measurement of the attenuation of the variable attenuator whereby the maximum damping was reached here. In the first plot, the voltage is plotted versus time. In the second plot, the voltage is compared to the noise and in the third plot, the voltage versus time is plotted versus the calculated power.

The achieved attenuation is plotted in figure 24 over the different measurement points.

| Measurement | Voltage mean [V] | Power mean [W] | Attenuation [dB] |
|---|---|---|---|
| 1. measurement | $11.783 \pm 0.038$ | $2.009 \cdot 10^{-8} \pm 3.543 \cdot 10^{-12}$ | ——— |
| 2. measurement | $7.046 \pm 0.033$ | $1.202 \cdot 10^{-8} \pm 4.430 \cdot 10^{-11}$ | $-2.232 \pm 0.037$ |
| 3. measurement | $4.049 \pm 0.0178$ | $6.904 \cdot 10^{-9} \pm 1.997 \cdot 10^{-11}$ | $-4.640 \pm 0.029$ |
| 4. measurement | $0.992 \pm 1.780 \cdot 10^{-3}$ | $1.693 \cdot 10^{-9} \pm 6.705 \cdot 10^{-12}$ | $-10.744 \pm 0.041$ |
| 5. measurement | $0.062 \pm 4.432 \cdot 10^{-4}$ | $9.634 \cdot 10^{-12} \pm 1.307 \cdot 10^{-13}$ | $-33.192 \pm 0.137$ |
| 6. measurement | $0.061 \pm 8.454 \cdot 10^{-4}$ | $9.472 \cdot 10^{-12} \pm 1.369 \cdot 10^{-13}$ | $-33.266 \pm 0.146$ |
| 7. measurement | $0.055 \pm 2.179 \cdot 10^{-4}$ | $8.410 \cdot 10^{-12} \pm 1.55 \cdot 10^{-13}$ | $-33.790 \pm 0.186$ |

Table 2: In this listing table the results, as well as the calculated values of the measurement series for the determination of the attenuation of the variable attenuator are written down.

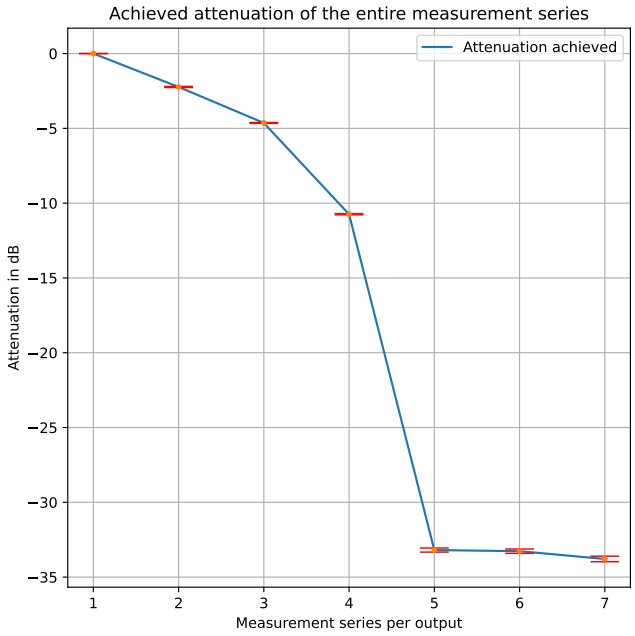


Figure 24: Attenuations of the power of the laser plotted over the individual measurement series. The error bars are hardly visible because the errors are too small as seen in table 1 .

It can be seen that, as expected, the power continues to decrease as the attenuation is increased. At the end of the measurement series, an attenuation of $-33.790 \pm 0.186$ dB is reached, this is expected due to measurement series by Dr. Manuel Meyer (28.43 dB) [25] that had already been completed in the past. Measurements 6 and 7 are very similar, since both were measured at the edge of the photodiode's sensitivity. Since for measurements 6 and 7 it was necessary to change to high gain and Channel 2 $\pm$ 1V, a different noise was also used than for the previous measurements. However, these noise measurements are negative, so they were not subtracted from the measured values but added.

## 4.2 Procedure to determine the attenuation factor: a step-by-step guide

Based on the experience of the previous measurements, the following guide describes the recommended step-by-step procedure for detemining the attenuation of the variable attenuator and thereby the power sent to the TES.

### 4.2.1 Recommended step-by-step procedure for detemining the attenuation of the variable attenuator

1. The first measurement should be performed with the entire setup and the laser turned off to measure the noise of the experimental setup. This should be done for 5 minutes each for channel 1, $\pm$20 V and for channel 2, $\pm$1 V in high gain and low gain.

   (a) Laser settings: Switched off

   (b) Settings SK Attenuator Block: Fully open

   (c) Settings variable attenuator: Fully open

   (d) Photodiode setting: Low gain and high gain

   (e) Setting Red Pitaya: Channel 1 $\pm$20 V, channel 2, $\pm$1 V

   (f) Recommended measuring time 5 min

2. Then the laser should be turned on and run for 2-3 hours to avoid fluctuations.

   (a) The general conditions (the room temperature, the temperature of the materials [especially the Red Pitaya, since it heats up a lot], the setup, the location of the cables) should be almost the same throughout the test. **Therefore, steps 1 and 2 should follow each other immediately.**

3. The following measurements should be performed at constant attenuation which means that the screw of the attenuator should always be kept in the same position. It is recommended that the attenuator setting be changed before the actual measurement so that the desired measuring range is achieved, and only then carry out the actual measurement. What practically means that an intermediate measurement should be made with the Red-Pitaya, in which the next larger attenuation step is set, so that no manually generated fluctuations are measured in the recorded series of measurements, but values that are as constant as possible. Then a new measurement series should be started at the selected attenuation, which is then saved.

4. To reconstruct the damping in the actual test setup in the TES, the rotation of the screw on the variable attenuator should be measured or the position of the screw must not be changed from the maximum attenuation values reached. However, this is only possible under the same general conditions.

5. Determine the maximum power of the laser so that the calPD is not saturated. This will be the value $P_0$ used equation 4.1.3 to determine the damping factor.

   (a) Laser settings: Switched on

   (b) Settings SK Attenuator Block: turned up to the point where the maximum power at the calPD is reached, without saturating the device. The calPD saturates at 12 V, so open the attenuator cube to the point where it is as close to 12 V as possible, without fully reaching 12 V (e.g. 11.8 V). This should be done using an oscilloscope and watching the output voltage as the knob is opened/closed. From this point on, the Attenuator Block should not be adjusted any further.

   (c) Photodiode setting: Low Gain

   (d) Setting Red Pitaya: Channel 1 $\pm$20 V

   (e) Settings variable attenuator: Fully open

   (f) Recommended measuring time 5 min

6. **This can be done optionally.** Alternatively, you can skip directly to step 7. 2-3 measurements (in the range of 10 - 2 volts) should follow, during each of which the power of the laser is further attenuated. For each new measurement, the attenuation must first be adjusted and then measured at constant attenuation.

   (a) Laser settings: Switched on

   (b) Settings SK Attenuator Block: Unchanged, as described in step 6.

   (c) Photodiode setting: Low gain

   (d) Setting Red Pitaya: Channel 1 $\pm$20 V

   (e) Recommended measuring time 5 min

7. Another 2-3 measurements follow until the lower limit of the photodiode is reached. This is now the maximum attenuation that can be measured. (From 1 Volt measurement in the calPD, the Channel 1 $\pm$ 20V must be changed to Channel 2 $\pm$ 1V). The power $P$ measured or calculated (see equation 4.1.2) here is then measured in relation to $P_0$ (see equation 4.1.3).

   (a) Laser settings: Switched on

   (b) Settings SK Attenuator Block: Unchanged, as described in step 6.

   (c) Photodiode setting: High gain

   (d) Setting Red Pitaya: Channel 2 $\pm$1 V

   (e) Recommended measuring time 5 min

8. This measurement data of the attenuation must then be subtracted by the corresponding noise measurment in step 1, keeping in mind whether the measurment was done with Channel 1 or Channel 2 of the RedPitaya, and on whether the calPD was set to High or Low gain, to achieve the actual results.

# 5 Discussion of the Errors

In this section, the results and errors are shown and possible causes are discussed.

## 5.1 Discussion about the test of the stability of the laser

The laser stability as seen in Figure 16 is not constant, but fluctuates over larger time intervals as already described in Results section 4.1.1. Possible sources of error can be fluctuations in the power grid. There could have been a sudden voltage drop at about 2.5 hours, but this is not traceable. Also, the increase in power from hour 16 could be due to a change in the grid voltage. Another possibility is the change in room temperature. The measurement was done over night and the increase could have been due to other people working and thus an increase in temperature in the room. However, no work is logged that should lead to a strong increase in room temperature. The cause of the fluctuation therefore remains largely unexplained. Another possibility would be the increase of the temperature of the laser diode itself. It can be observed that the power of the laser increases linearly with time and is below the average value from 0 to about 6 hours and significantly above the average value from 15 hours.

## 5.2 Discussion about the determination of the dark noise of the entire experimental setup

In general, it can be said that the noise is result of the electronic noise of the experimental setup (see figure 13) itself. Whereby the calPD and the RedPitaya probably have the largest contribution to the noise and thus represent the largest sources of error
The noise measurements are very different as can be seen in the section 4.1.2. In addition, movement on the experimental setup (see section 3) can cause the measurement to change. However, during the measurement, care was taken not to touch the experiment.

During the measurement for the noise in the Channel 1 $\pm$ 20V in low gain (see figure 17), fluctuations in the mV range $0.03 \pm 0.002$ V are observed. The fluctuations could be due to temperature differences in the laboratory and to the intrinsic temperature of the experimental setup (see section 3). The temperature of the room did not change much during the measurement. However, the RedPitaya heated up strongly during operation and could have an influence measurements. However, the extent of the change in the measured values due to the movement of the experimental setup was not determined.

In the measurement for the noise in the Channel 1 $\pm$ 20V in high gain (see figure 18), similar fluctuations as in the Channel 1 $\pm$ 20V in low gain, in the range $-0.06 \pm 0.002$ V can be observed. Reason for this could be the same as described for Channel 1 low gain. Presumably, the negative values can be explained by the undercutting of the sensitivity of the photodiode. If the input falls below a certain value ($\approx$ 0.01V), the photodiode can no longer measure the power

and outputs negative values instead. It can be observed that the negative value increases linearly with higher attenuation. Since there is uncertainty about the interpretation of the negative values, the attenuation was only measured up to the limit ($\approx 0.01V$). In fact, the photodiode only shows negative values when the current reverses. However, this did not happen and the reason for the negative values cannot be determined. The standard deviation for Channel 1 $\pm$ 20V in high gain and for Channel 1 $\pm$ 20V in low gain are small and thus the fluctuations are not very large.

When measuring for noise in Channel 2 $\pm$ 1V in low gain (see figure 19), there are fluctuations in the range $-0.01 \pm 0.00004$ and when measuring for noise in Channel 2 $\pm$ 1V in high gain (see figure 20), there are fluctuations in the range $-0.10 \pm 0.0002$. In addition, both values are negative. The reason for these fluctuations and the negative values is probably the same as described for Channel 1 $\pm$ 20V in high gain. The standard deviation for Channel 2 $\pm$ 1V in low gain and Channel 2 $\pm$ 1V in high gain are small and thus the fluctuation is not large. The negative values can also just be an offset from ground. Maybe somehow the grounds of the devices are not in line with each other, leading to an offset.

The expected energy per time Blackbody radiation in a wavelength range of $\lambda = 500nm - 2000nm$ is $4.05 \cdot 10^{-17}W$ (see equation 4.1.9). The noise, on the other hand, lies in a range from $1.1 \cdot 10^{-11}W$ to $6 \cdot 10^{-11}W$ (see table 1). It can be seen that the blackbody radiation cannot have a big influence on the calPD, because the value is much smaller than the received noise. Thus, the blackbody radiation can be neglected.

## 5.3 Discussion about the light pollution test

The purpose of the measurements of the Light pollution test (see section 4.1.4) was to check whether the light in the room had an influence on the measurements. According to the evaluation of the measurement results, the light has no influence within the sensitivity of the measurement devices. The measurement results are very similar in the mean value, as well as in the standard deviation and the fluctuations can be explained with the explanation from section 5.2.

## 5.4 Discussion about the measurements of the attenuation of the variable attenuator

In general, it can be observed that all measured values in the section 4.1.5 are subject to slight fluctuations. However, these fluctuations do not deviate strongly from the mean value (see standard deviation 2) and therefore the measurement series can be evaluated as usable. The temperature in the room probably had a large influence on the measured values, because it extended the attenuator and led to partly strongly different measurements (temperature fluctuations by neighboring experiments in the room (cryostat of the TES, etc.)). The temperature

changes could not be measured in the room, so this source of error remains only a conjecture and cannot be evaluated. Also movements of the optical fibers led to sometimes strongly different measurements. These observations led to the conclusion that the measured values are not reproducible and therefore the attenuation of the attenuator must be redetermined for each new sensitivity measurement. See the recommended manual (section 4.2.1).

Another source of error was the inaccurate setting of the variable attenuator. Only a small screw could be turned with the fingers, without the possibility to measure the rotation. Adjustment by hand also proved to be difficult, as even the slightest movement of the screw could cause large changes in attenuation. This was especially obvious when approaching the saturation limit of the photodiode. It was hardly possible to achieve even better attenuation, since it was not possible to move the screw more precisely by hand. This also contributes to the fact that the measurement series are not reproducible.

The errors of all measurement series are small. They are on average in voltage $0.1\%$ and in power $0.1\% - 0.01\%$, as well as in attenuation $1\% - 0.1\%$ (see table 2). The achieved value of the attenuation (see figure 24) is close to the expected value and therefore the experimental setup for the determination of the attenuation (see figure 13) can be used for further experimental steps.

# 6 Summary

In summary, the experiment can be considered a success and the task as fulfilled. The expected attenuation of $\approx -34$ dB was achieved and a manual was created with which the measurement series can be repeated.

The results of the laser stability measurement suggest that the laser must be turned on at least 2 hours before measuring the efficiency of the TES, so that the laser has a stable output. The reason for the fluctuations remains unclear and can only be speculated. However, since the fluctuations only occur over a large period of several hours and the calibration of the test takes less than 30 minutes, the fluctuations in the power of the laser should not cause any problems in the measurement.

The dark noise of the experimental setup was not very strong and is partly below the sensitivity of the photodiode. Therefore, it can be assumed that the experimental setup is suitable for measuring the attenuation of the variable attenuator. The origin of the negative measurement data remains unclear. However, this data was treated in the calculations in such a way that the negative value does not cause any problems. For the measurement series of the attenuation and the accompanying conversions, only the noise in Channel 1 $\pm$ 20V in low gain and in Channel

$2 \pm 1$V in high gain were used.
The test on the light pollution of the measurement series by the ceiling light in the laboratory was concluded with the result that the light has no influence on the measurements. Rather, temperature, voltage changes in the electrical supply lines and movements on the light guides play a role.

The measurements of the attenuation of the variable attenuator were successful in that they achieved an attenuation of $\approx -34$ dB, as mentioned earlier. However, reaching the lowest measurement limit proved to be difficult, in that the adjustment of the variable attenuator screw had to be extremely precise. Thus, there was difficulty in achieving a higher attenuation. Another method is recommended to turn the screw and measure its rotation. One possible method would be a rotation angle measuring device.

# 7 Outlook

The achieved attenuation of $\approx 34$ dB can now be used for the determination of the efficiency of the Transition Edge Sensor (TES) to verify the losses in the TES (see section 1.4). Now that it has been determined how strong the damping of the variable attenuator is in the $99\%$ line, the damping in the $1\%$ line, which is used to set up the efficiency measurement (see section 1.4), can be calculated.
The thus determined efficiency of the TES is then taken into account when running the ALPS experiment (see section 1.2) and it can be started to search for the Axion.

# 8 Bibliography

# References


[1] D P Clemens. Massachusetts-Stony brook galactic plane CO survey - the galactic disk rotation curve. *Astrophys. J.*, 295:422, August 1985.

[2] F. Zwicky. Die Rotverschiebung von extragalaktischen Nebeln. *Helvetica Physica Acta*, 6:110–127, 1933.

[3] Galaxies behind a gravitational magnifier. JULY 28, 2022.

[4] P. Tisserand et al. Limits on the Macho Content of the Galactic Halo from the EROS-2 Survey of the Magellanic Clouds. *Astron. Astrophys.*, 469:387–404, 2007.

[5] Ahmed Tarek Abouelfadl Mohamed. *The Standard Model of Particle Physics*, pages 3–35. Springer International Publishing, Cham, 2020.

[6] Candida S. Punla, https://orcid.org/ 0000-0002-1094-0018, cspunla@bpsu.edu.ph, Rosemarie C. Farro, https://orcid.org/0000-0002-3571-2716, rcfarro@bpsu.edu.ph, and Bataan Peninsula State University Dinalupihan, Bataan, Philippines. Are we there yet?: An analysis of the competencies of BEED graduates of BPSU-DC. *International Multidisciplinary Research Journal*, 4(3):50–59, September 2022.

[7] Sandbox Studio. Doe explains...the standard model of particle physics.

[8] Leszek Roszkowski, Enrico Maria Sessolo, and Sebastian Trojanowski. WIMP dark matter candidates and searches—current status and future prospects. *Rept. Prog. Phys.*, 81(6):066201, 2018.

[9] A. Ringwald. Axions and Axion-Like Particles. In *49th Rencontres de Moriond on Electroweak Interactions and Unified Theories*, pages 223–230, 2014.

[10] J. Guenther S. Borsanyi, Z. Fodor. Calculation of the axion mass based on high-temperature lattice quantum chromodynamics. 2016.

[11] Klaus Ehret, Maik Frede, Samvel Ghazaryan, Matthias Hildebrandt, Ernst-Axel Knabbe, Dietmar Kracht, Axel Lindner, Jenny List, Tobias Meier, Niels Meyer, Dieter Notz, Javier Redondo, Andreas Ringwald, Günter Wiedemann, and Benno Willke. New ALPS results on hidden-sector lightweights. *Physics Letters B*, 689(4-5):149–155, may 2010.

[12] P. Sikivie. Experimental tests of the "invisible" axion. *Physical Review Letters*, 51(16):1415–1417, oct 1983.

[13] A. A. Anselm. Experimental test for arioni⇆/iphoton oscillations in a homogeneous constant magnetic field. *Physical Review D*, 37(7):2001–2004, apr 1988.

[14] K. Van Bibber, N. R. Dagdeviren, S. E. Koonin, A. K. Kerman, and H. N. Nelson. Proposed experiment to produce and detect light pseudoscalars. *Physical Review Letters*, 59(7):759–762, aug 1987.

[15] R. D. Peccei and Helen R. Quinn. Constraints imposed by CP conservation in the presence of pseudoparticles. , 16(6):1791–1797, September 1977.

[16] R. D. Peccei and Helen R. Quinn. CP conservation in the presence of pseudoparticles. , 38(25):1440–1443, June 1977.

[17] Leanne D Duffy and Karl van Bibber. Axions as dark matter particles. *New J. Phys.*, 11(10):105008, October 2009.

[18] Rikhav Shah. A TES Detector for ALPS II. 2021.

[19] Robin Bähre et al. Any light particle search II —Technical Design Report. *JINST*, 8:T09001, 2013.

[20] R Bähre, B Döbrich, J Dreyling-Eschweiler, S Ghazaryan, R Hodajerdi, D Horns, F Januschek, E A Knabbe, A Lindner, D Notz, A Ringwald, J E von Seggern, R Stromhagen, D Trines, and B Willke. Any light particle search ii — technical design report. *Journal of Instrumentation*, 8(09):T09001, sep 2013.

[21] Julian Dietz. Thermal effects in the detection of single photons, 2021.

[22] Jan Dreyling-Eschweiler. *A superconducting microcalorimeter for low-flux detection of near-infrared single photons*. PhD thesis, U. Hamburg, Dept. Phys., 2014.

[23] Recommended procedure for the efficiency measurement.

[24] Katharina-Sophie Isleif. Confluence at DESY, System detection efficiency.

[25] Confluence at DESY, Lab Updates 12.08.2022: Setup for efficiency measurements and a first look at the variable attenuator.

# 9 Acknowledgment

I would like to thank Dr. Manuel Meyer and especially Dr. Gulden Othman, who supervised me very well throughout the entire Bachelor thesis. Thanks to their care and patience, as well as constructive criticism and helpful suggestions, I was able to successfully complete the bachelor thesis.

Furthermore, I would like to thank the ALPS-TES detector team, as they always supported me with words and deeds.

In addition, I would also like to thank Dr. Jonas Siegel and the team of Lights & School, as I was always able to come to them with open questions and received a lot of support.

In particular, I would also like to thank the University of Hamburg and the German Electron Synchrotron for providing me with space and materials.

Last but not least, I would like to thank my whole family, without their huge support and understanding, I would never have come this far.

# 10 Statutory declaration

I certify that I have prepared the enclosed written Bachelor's thesis independently and have not used any auxiliary materials other than those indicated.
All passages that are taken from other works in terms of wording or meaning, I have in each case clearly indicated the source as borrowing. This also applies to all information taken from the Internet or other electronic data other electronic data collections.
I further declare that the Bachelor's thesis I have written in the same or a similar version has not yet been part of a course of study or examination within the framework of my studies. course of study. The written version submitted by me corresponds to the one on the electronic storage medium.

I hereby agree that my Bachelor thesis can be published.

Stelle, 21.12.2022
Place, Date

Jan Wiesenmüller
Signature

# A Appendix

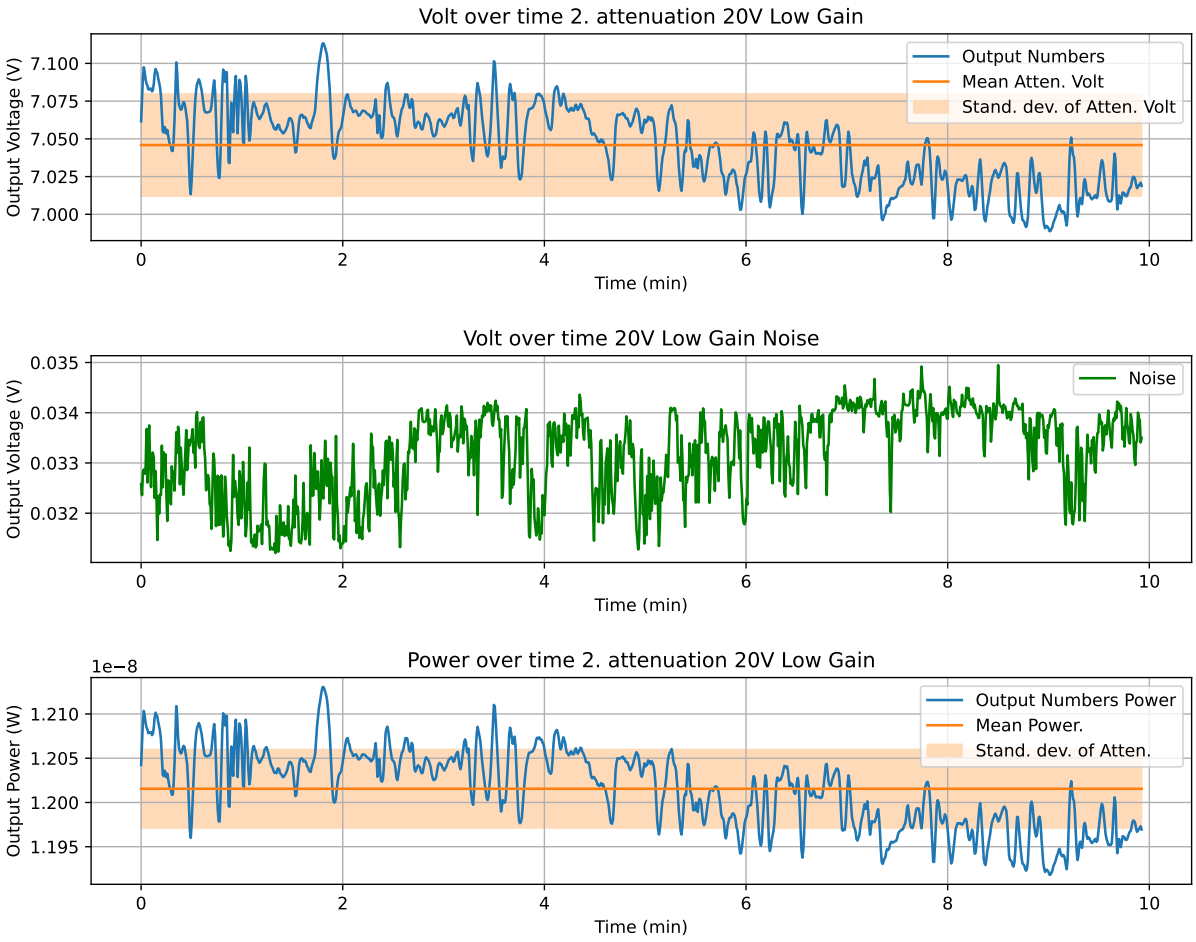


Figure 25: The second measurement of the attenuation of the variable attenuator. In the first plot, the voltage is plotted versus time. In the second plot, the voltage is compared to the noise and in the third plot, the voltage versus time is plotted versus the calculated power.

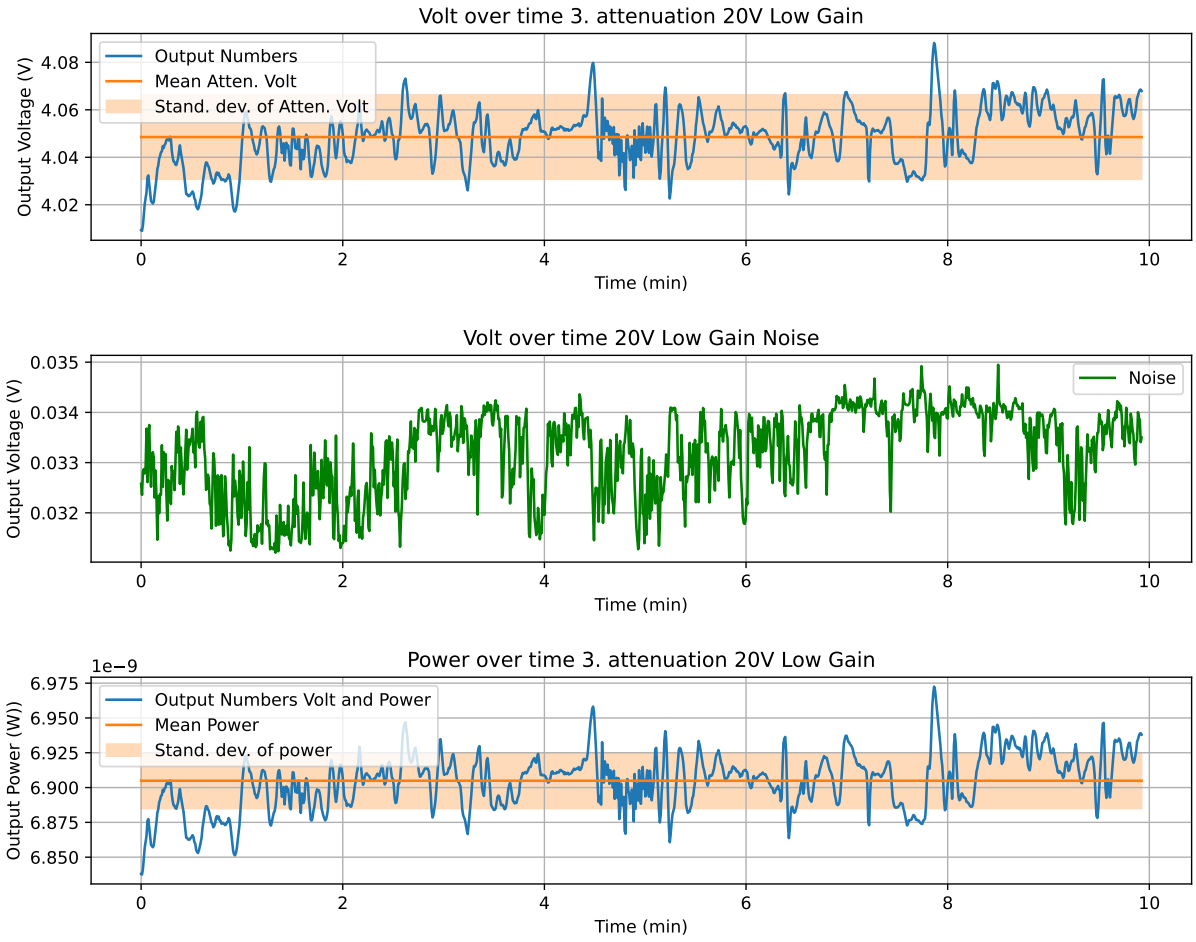


Figure 26: The third measurement of the attenuation of the variable attenuator. In the first plot, the voltage is plotted versus time. In the second plot, the voltage is compared to the noise and in the third plot, the voltage versus time is plotted versus the calculated power.

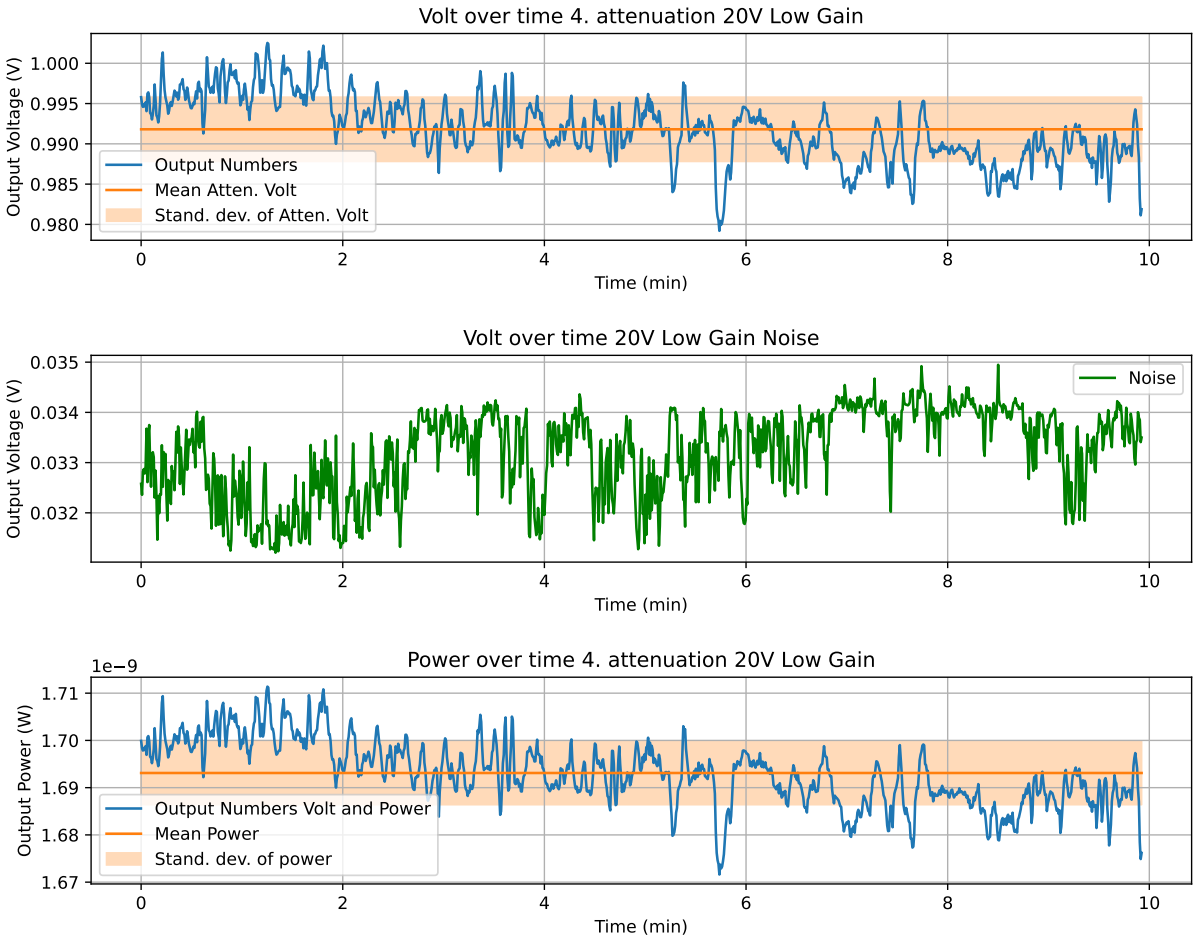


Figure 27: The fourth measurement of the attenuation of the variable attenuator. In the first plot, the voltage is plotted versus time. In the second plot, the voltage is compared to the noise and in the third plot, the voltage versus time is plotted versus the calculated power.

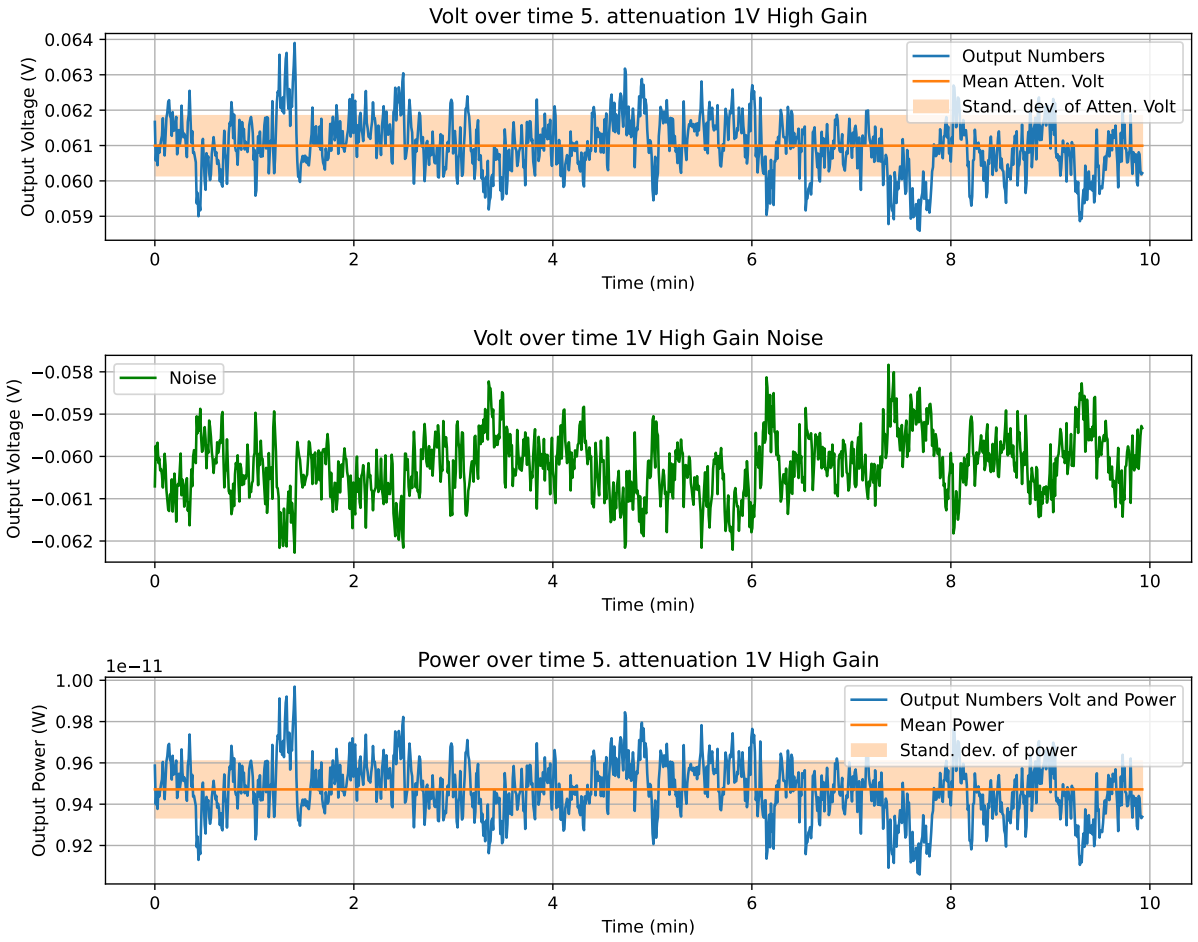


Figure 28: The fifth measurement of the attenuation of the variable attenuator. In the first plot, the voltage is plotted versus time. In the second plot, the voltage is compared to the noise and in the third plot, the voltage versus time is plotted versus the calculated power.


Figure 29: Me at the ALPS II experiment

Figure 30: Me at the Hera tunnel